Journal of Testing and Evaluation, Vol. 31, No. 1
Paper ID JTE11402_311
Available online at: www.astm.org

Monika G. Garrell,[1] Albert J. Shih,[2] Edgar Lara-Curzio,[3] and Ronald O. Scattergood[4]

Finite-Element Analysis of Stress Concentration in ASTM D 638 Tension Specimens

ABSTRACT: Experimental results showed that ASTM D 638 Type IV flat tension specimens, made of a Nylon-11 matrix containing a large volume concentration of Nd-Fe-B particulates, failed at a location where the straight gage section of the specimen ends and the curved transition region begins. The stress distribution in this specimen was analyzed using the finite-element method, and it was found that there is a stress concentration at this location. The stress distributions in tension specimens with both single- and double-arc transition regions were analyzed and stress concentration factors were calculated. A linear relationship between the magnitude of the stress concentration factor and the ratio of the width in the gage section and the arc radius of the transition region is identified. This study shows that it is possible to reduce the magnitude of the stress concentration factor for the ASTM D 638 Type IV flat tension specimen by redesigning the specimen geometry without changing its overall size.

KEYWORDS: stress concentration factor, finite-element analysis, tensile strength

Recent advancements in injection molding have made it a popular manufacturing method for cost-effective, high-volume production of plastic and particle-reinforced plastic composites. ASTM Standard D 638 [1], a standard test method for tensile strength of plastics, has been used widely in the industry to evaluate the tensile strength of plastic-based materials. In the absence of test methods for the tensile evaluation of particulate-reinforced plastics, the ASTM D 638 test method also has been used to evaluate these reinforced plastic composites. Figure 1*a* shows a fractured ASTM D 638 Type IV specimen made of Nylon-11 bonded Nd-Fe-B particles. This material, which contains 59.7 vol% of brittle Nd-Fe-B particles, is formulated for permanent magnet applications. The high percentage of Nd-Fe-B particles is necessary to achieve the desired magnetic properties for electrical motor and actuator applications. However, the high percentage of Nd-Fe-B particles also results in a material with reduced ductility [2–4].

The tensile evaluation of plastic-bonded Nd-Fe-B magnets has shown that fracture almost always initiates at a location where the straight gage section of the specimen ends and the curved transition region begins. This location is marked as Point B in Fig. 1*a*. The failure at Point B, which is outside the uniformly loaded straight gage section, is due to a stress concentration and can lead to an underestimate of the tensile strength. Such stress concentration is not a problem for ductile materials because the large plastic deformation will redistribute the stress. For example, Fig. 1*b* shows a deformed ASTM D 638 Type IV tension specimen made of pure Nylon-11. This specimen continued to deform extensively without fracturing at the location of initial stress concentration.

Manuscript received 5/2/2002; accepted for publication 11/13/2002; published 11/18/2002.

[1] Department of Mechanical and Aerospace Engineering, North Carolina State University, Raleigh, NC 27695.

[2] Department of Mechanical Engineering, University of Michigan, Ann Arbor, MI 48109.

[3] High Temperature Materials Laboratory, Oak Ridge National Laboratory, Oak Ridge, TN 37831.

[4] Department of Materials Science and Engineering, North Carolina State University, Raleigh, NC 27695.

As engineered and particle-reinforced plastics become stronger and in some cases more brittle, the stress concentration in current tension specimen geometries has become an issue of concern. One of the objectives in this research is to analyze the stress concentration factor [5] on specimens specified in ASTM D 638 using the finite-element method. Five types of specimens, designated as Type I, II, III, IV, and V, are defined in ASTM D 638. The shapes of Type III and V specimens are similar, which results in the same stress concentration factor at the location where the gage section ends and the transition region begins. Therefore, only Type I, II, III, and IV specimens were studied. In addition to these four standard tension specimens, the stress concentration factor for other specimen geometries with single- or double-arc fillets was also analyzed using the finite-element method to investigate possible ways to reduce the stress concentration without changing the overall size of specimens.

The photoelastic method has been used in the past to study the stress concentration factors for shoulder fillets in flat plates [5–7]. Most of the cases studied have fillet radii much smaller than the width of the specimen. The shapes of tension specimens investigated in this research have the opposite trend: the fillet radii are much larger than the width of the specimen in order to reduce the stress concentration factor. For specimens with very small stress concentration factors, the finite-element method with a reasonably fine mesh was applied to analyze the stress distributions and estimate the stress concentration factors. The finite-element method has been applied previously to the design of flat tension specimens of advanced composites [8], ceramic matrix composites [9], and monolithic ceramics for creep testing [10]. Oplinger et al. [11] has studied the use of streamlined specimens to reduce the tensile and shear stress concentration in composite specimens.

In this paper, first the finite-element modeling of tension specimens is introduced. The stress concentration factor is defined. The distribution of von Mises stresses for four types of specimens specified in ASTM Standard D 638 is presented. The stress concentration factors of other specimen shapes with single- and double-arc fillets are analyzed. Finally, a correlation between the magnitude of the stress concentration factor and the ratio of arc radius and width of the gage section is established.

Finite-Element Modeling

The two-dimensional plane stress six-node and twelve degree-of-freedom triangular linear elastic element was selected to model the flat-plate tension specimens. The commercially available ANSYS finite-element analysis software and its mesh generator were used. Figure 2 shows the finite-element meshes used to model the four types of ASTM D 638 tension specimens.

Due to the symmetry of the specimen geometry, only one quarter of the specimen is modeled. Point O is the center of the specimen. Lines OA and OE are the symmetry planes of the specimen. Point O is fixed in both the X- and Y-directions. Nodes on Line OA have zero displacement in the X-direction and are free to move in the Y-direction. Nodes on Line OE have zero displacement in the Y-direction and are free to move in the X-direction. Nodes on Line ED are prescribed a uniform 0.1-mm displacement in the X-direction and zero displacement in the Y-direction. This is intended to simulate the holding of both ends in the wide section of the tension specimen using perfectly rigid grips. The extension of the specimen under this condition is 0.2 mm. In actual tensile tests, the specimen is clamped and pulled using a set of mechanical or hydraulic grips. The actual loading condition near the gripped area is therefore the combination of the normal compressive stress and in-plane tensile and shear stresses.

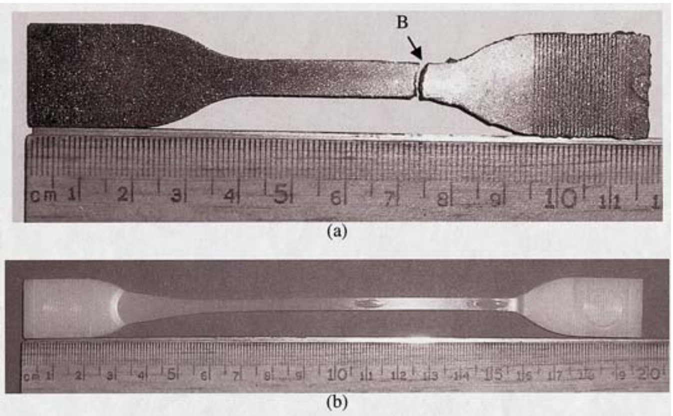

FIG. 1—*Pictures of ASTM D 638-98 Type IV tension specimens: (a) Nylon-11 bonded Nd-Fe-B (59.7 vol%) material tested with at 100°C, and (b) pure Nylon-11 tested at 100°C.*

Dimensions of finite-element meshes and the number of elements and nodes are summarized in the table in Fig. 2 for each type of ASTM D 638 specimen. OA is one half of the width of the gage

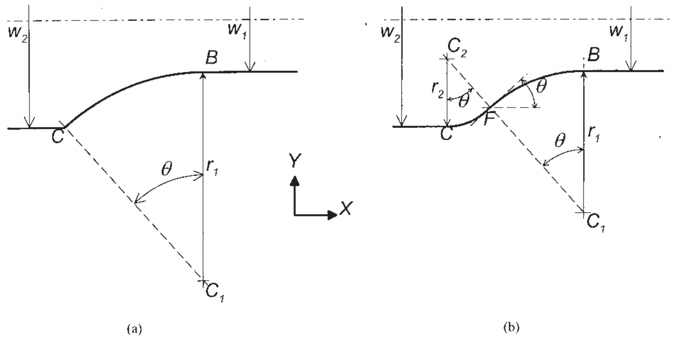

FIG. 3—*Geometric model of the single and double radius transitional area.*

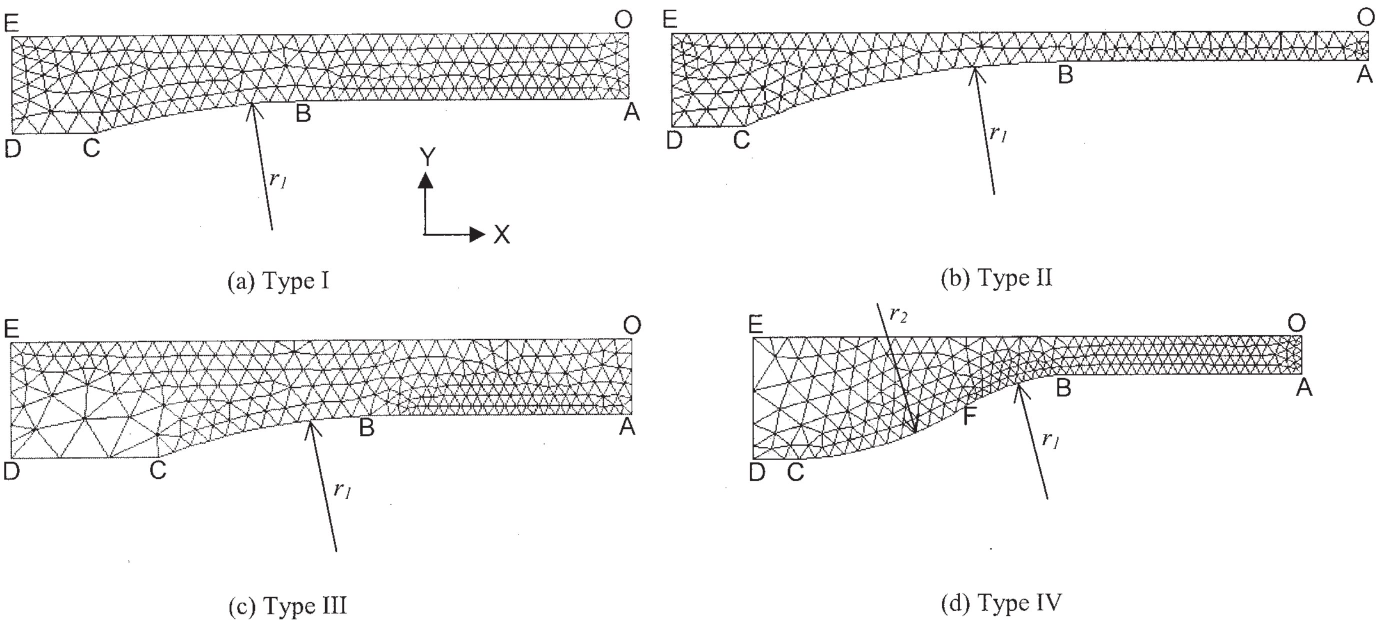

	Number of Elements	Number of Nodes	OA (mm)	AB (mm)	CD (mm)	DE (mm)	OE (mm)
Type I	375	316	6.5	28.5	7.86	9.5	57.0
Type II	263	278	3	28.5	7.25	9.5	66.5
Type III	441	349	9.5	28.5	12.39	14.5	73.0
Type IV	438	367	3	16.5	2.44	9.5	40.5

FIG. 2—*Finite-element mesh for four types of specimen in ASTM D 638-98.*

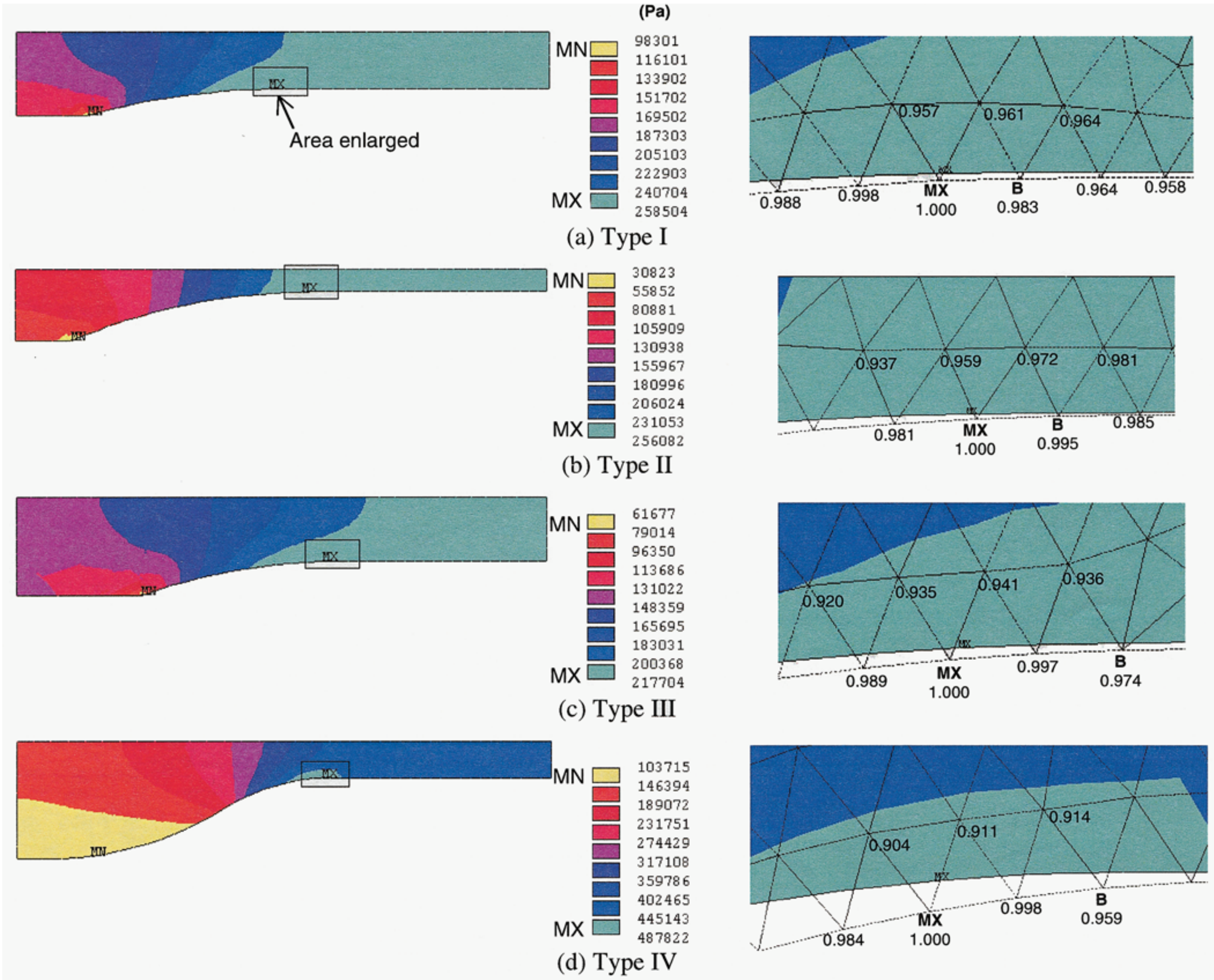

FIG. 4—*Distribution of von Mises stress in ASTM D 638 tensile test specimens. (Value by the node represents the ratio of nodal von Mises stress relative to the maximum von Mises stress at node MX in Pa.)*

section, DE is one half of the width of the wide section, OE is one half of the length of the specimen, and AB is one half of the length of the gage section. Between Points B and C, the specimen changes from the narrow to the wide section. As shown in Figs. 2*a*, 2*b*, and 2*c*, Type I, II, and III specimens consist of a circular arc of radius r_1 between Points B and C. These are known as single-arc specimens. As shown in Fig. 2*d*, two radii, r_1 and r_2, are used to blend two arcs in the transitional region between Points B and C for the Type IV specimen. This is designated as the double-arc specimen.

The geometrical relationships of the single- and double-arc shape between Points B and C are shown in Fig. 3; w_1 and w_2 are widths of the narrow and wide section, respectively. As shown in Fig. 3*a*, the single-radius specimen has a continuous slope at Point B and a discontinuous slope at Point C. The double-arc specimen, as shown in Fig. 3*b*, has a continuous slope at all three transitional points: B, F, and C. Arcs BF and FC have the same angle, indicated by θ. The center of Arc BF, denoted as C_1 in Fig. 3*a*, has the same X-coordinate as Point B. Similarly, the center of Arc CF, denoted as C_2, has the same X-coordinate as Point C. These geometrical constraints together ensure a continuous slope at Points B, F, and C for the double-arc specimen.

A hydrostatic stress-dependent yield criterion is usually used to analyze stress concentrations in plastics [12,13]. The yield criterion for magnetic particle reinforced plastics has not yet been studied. The maximum von Mises stress was used to calculate the stress concentration factor and to identify the location that possibly initializes the fracture. In addition to the von Mises stress, the maximum principal stress, which is more suitable for the analysis of brittle materials, was also applied to calculate the stress concentration factor.

The finite-element analysis provided results of stress components and the von Mises and principal stress for each node. The nodal stress was used to calculate the stress concentration factor, K_f.

$$K_f = \frac{\sigma_{max}}{\sigma_{nominal}} \tag{1}$$

where σ_{max} is either the maximum nodal von Mises stress or maximum first principal stress, and $\sigma_{nominal}$ is either the average von Mises stress or the average first principal stress on nodes in the gage section. Finite-element analysis results show that the variation of von Mises stress among nodes in the gage section is very small, less than 1.5%. An elastic modulus of 130 MPa and Poisson's ratio of 0.3 were used in the finite-element analysis.

Finite-Element Analysis of Four Types of Tension Specimens

Figure 4 shows the distribution of von Mises stress for ASTM D 638 Type I, II, III, and IV standard tension specimens. For each specimen, an overview and another enlarged view of the von Mises stress distribution is presented. The enlarged view is centered about Point B to identify the increase in von Mises stress. In Fig. 4, MX and MN mark the nodes with maximum and minimum von Mises stress, respectively. As shown in the overview of the specimen, Node MN is close to Point C. In the enlarged view, the location of Node MX relative to Node B can be seen. Node MX is next to Node B, as in Type I and II, or a node away from Node B, as in Type III and IV. It is noted that the mesh shown in the enlarged view represents the exaggeratedly deformed finite-element mesh from the ANSYS output. Node B, originally located at the intersection of a straight line and an arc, can be seen on a slightly curved region after deformation.

TABLE 1—*The stress concentration for different single- and double-radius tension specimen geometry.*

	Designation	r_1 (mm)	r_2 (mm)	w_1/r_1	K_f
ASTM D 638	Type I	76.0	. . .	0.171	1.046
	Type II	76.0	. . .	0.079	1.014
	Type III	76.0	. . .	0.250	1.068
	Type IV	14.0	25.0	0.429	1.112
Single radius tension specimen	S-I	6.5	. . .	0.923	1.245
	S-II	9.0	. . .	0.667	1.174
	S-III	13.0	. . .	0.462	1.119
	S-IV	19.0	. . .	0.316	1.083
	S-V	28.0	. . .	0.214	1.056
	S-VI	39.0	. . .	0.154	1.040
	S-VII	52.0	. . .	0.115	1.030
Double radius tension specimen	D-I	9.0	30.0	0.667	1.181
	D-II*	14.0	25.0	0.429	1.112
	D-III	17.0	22.0	0.353	1.091
	D-IV	19.5	19.5	0.308	1.081
	D-V	22.0	17.0	0.273	1.072
	D-VI	25.0	14.0	0.240	1.061
	D-VII	30.0	9.0	0.200	1.051

* The same geometry as Type IV.

The ratio of nodal von Mises stress relative to the maximum von Mises stress at Node MX is also presented in the enlarged view on nodes around Points B and MX in Fig. 4. For Type I, II, and III specimens, the overview of von Mises stress distribution does not show the stress concentration. Upon closely examining the distribution of von Mises stress around Point MX in the enlarged view, all four types of ASTM D 638 tension specimens demonstrate different levels of stress concentration at Node MX.

The von Mises stress at Node MX (σ_{max}) and at nodes in the gage section ($\sigma_{nominal}$) were extracted from the finite-element output and substituted into Eq 1 to calculate the stress concentration factor, K_f. Results of K_f are listed in Table 1. Type IV and II specimens have the highest and lowest K_f, 1.112 and 1.014, respectively. It was found that K_f has an almost linear relationship versus the parameter w_1/r_1, as shown in Fig. 5, for the four types of ASTM D 638 specimen.

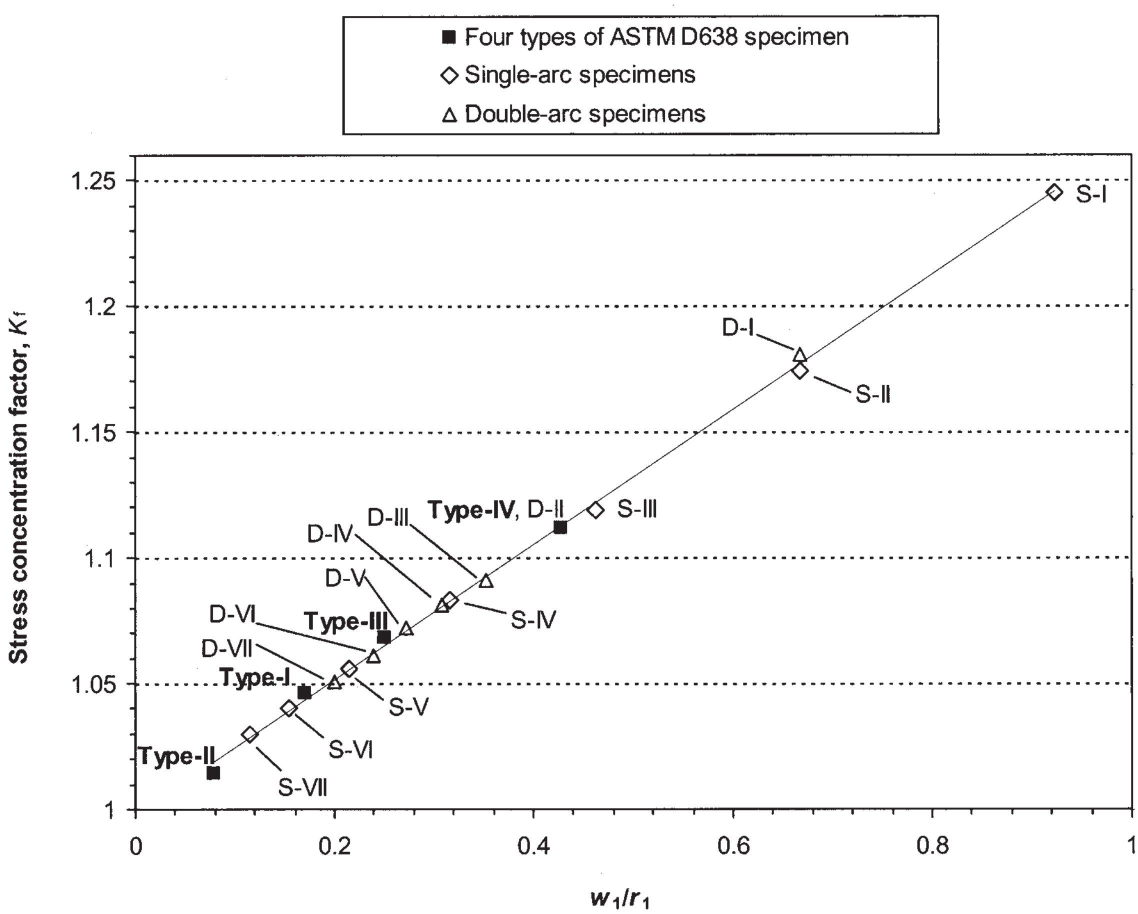

FIG. 5—*The stress concentration factor versus ratio of gage section width and radius for five types of ASTM D 638 specimens and the single- and double-radius specimens.*

Tension specimens with low w_1/r_1 ratio usually have large arc radius and are longer than specimens with high w_1/r_1. For example, as shown in Fig. 2 and Table 1, Type II and IV specimens have the same width in the gage section and different radius r_1. The Type II specimen has a larger arc radius, which makes the specimen longer and has lower w_1/r_1 and K_f. Longer and bigger tension specimens are unattractive because they require more material and a bigger die for injection molding and cost more to produce.

Instead of using the von Mises stress, the maximum principal stress and nominal principal stress were extracted from the finite-element output and substituted into Eq 1 to calculate K_f. For all four types of specimens, the difference in K_f based on von Mises and maximum principal stresses is very small, less than 0.001.

Finite-Element Analysis of Single- and Double-Arc Tension Specimens

In this section, the investigation of stress distribution in alternative tension specimen geometries that maintain the same overall size as the Type IV specimen is discussed. The objective is to identify the geometric parameters that would reduce the magnitude of K_f. The width (w_1) and length of the gage section are 6 and 13 mm, respectively. The width of the wide section, w_2, is 19 mm.

Two groups of sample geometry were studied. One group consists of single-arc specimens, similar to those in Type I, II, and III. Another group has the double-arc geometry, similar to the Type IV specimen.

Single-Arc Specimens

As shown in Table 1, seven single radius curves are used to blend between Points B and C. The minimum radius of Arc BC is 6.5 mm ($= (w_2 - w_1)/2$). The specimens with radii of 6.5, 9, 13, 19, 28, 39, or 52 mm at Arc BC were designated as S-I to S-VII, respectively. The shape and finite-element mesh of three selected specimens, S-I, S-IV, and S-VII, are shown in Fig. 6. For specimens with arc radius equal to or less than 39 mm, the overall length of the original Type IV specimen can be maintained. The K_f of the 39-mm radius single-arc specimen (S-VI), as shown in Table 1, is 1.040. This is significantly lower than K_f of 1.112 of the Type IV specimen.

Plots of K_f versus w_1/r_1 for these seven specimens are shown in Fig. 5. The larger radius of arc BC lowers both w_1/r_1 and K_f. Figure 5 also shows that the relationship between K_f and w_1/r_1 is almost linear and matches the trend of Type I to IV specimens.

Double-Arc Specimens

Seven double-arc specimens, denoted as D-I to D-VII, were studied as well. As shown in Fig. 3, the values of r_1 and r_2 in the double-arc geometry can be reversed and still maintain the continuity of both position and slope at Points B, F, and C. This special geometrical characteristic of the double-arc shape was used to define conjugate pairs of specimens. As shown in Table 1, D-I ($r_1 = 9$ mm, $r_2 = 30$ mm) and D-VII ($r_1 = 30$ mm, $r_2 = 9$ mm) form a conjugate pair of double-arc specimens. D-II ($r_1 = 14$ mm, $r_2 = 25$ mm) and D-VI ($r_1 = 25$ mm, $r_2 = 14$ mm) as well as D-III ($r_1 = 17$ mm, $r_2 = 22$ mm) and D-V ($r_1 = 22$ mm, $r_2 = 17$ mm) are another two sets of conjugate double-arc specimens. It is noted that the D-II specimen has the same geometry as the ASTM D 638 Type IV specimen. The intent is to investigate the change in K_f of a conjugate double-arc specimen. The D-III specimen has the same r_1 and r_2, both equal to 19.5 mm. The shape and finite-element mesh of three selected specimens, D-I, D-IV, and D-VII, are shown in Fig. 6.

Finite-element analysis results of K_f versus w_1/r_1 for seven double-arc specimens are listed in Table 1 and plotted in Fig. 5. It is important to note that the value of r_2 does not affect K_f. By just switching the two arcs of the original Type IV specimen, the K_f was reduced from 1.112 to 1.061. By further increasing r_1 to 30 mm without changing the overall size of the Type IV specimen, K_f was reduced to 1.051.

Modeling of the Stress Concentration Factor

As shown in Fig. 5, a straight line can be used to determine K_f for various w_1/r_1. Linear regression analysis was performed on all 17 data points, including the four types of specimen specified by ASTM D 638 and the seven single-arc and six double-arc specimens. The following model is obtained:

$$K_f = 0.268\,(w_1/r_1) + 0.998 \qquad (2)$$

Equation 2 can be used to predict the K_f based on w_1/r_1 and may be useful for new tension specimen design.

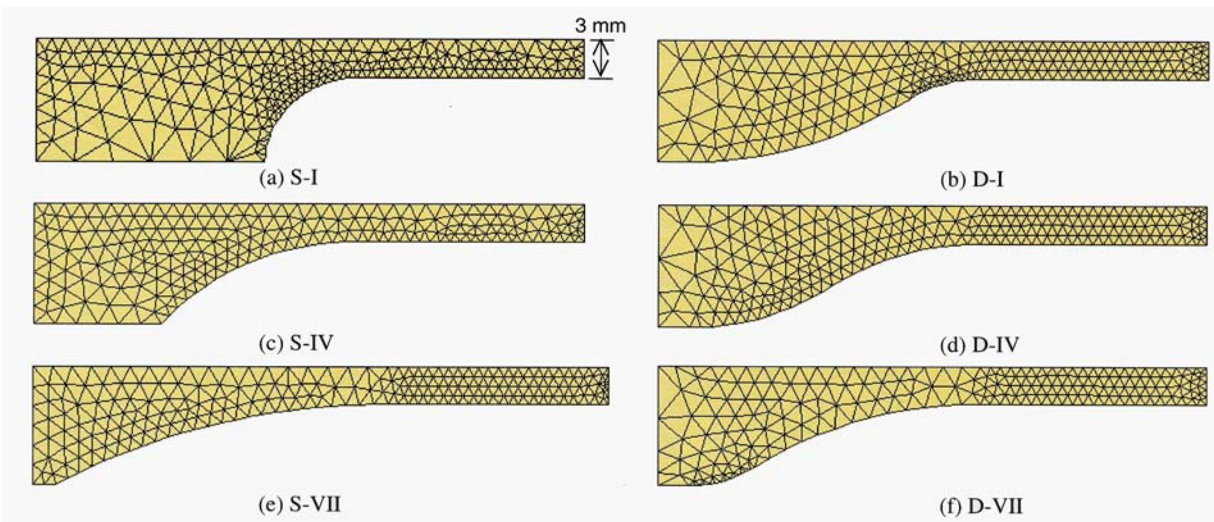

FIG. 6—*Finite-element meshes for selected single- and double-arc specimens (3 mm half-width in the gage section for all specimens).*

The linear trend indicates the possibility that an analytical solution for the stress distribution in this geometrical configuration may exist. This requires further investigation.

Concluding Remarks

The stress distribution of four types of tension specimens recommended in ASTM D 638 was investigated through the use of the finite-element technique. It was found that the location of maximum von Mises stress for Type IV geometry coincided with the location of experimentally observed failures in brittle specimens made of Nylon-11 bonded Nd-Fe-B particles. This study identified a solution to reduce the magnitude of stress concentration by increasing the radius of the arc in the transitional area. A linear correlation of stress concentration factor K_f versus w_1/r_1 was identified and a linear model was established to predict the K_f based on w_1/r_1. Results obtained in this research can help establish standards and aid in the design of specimen geometry for tension testing of brittle particle-reinforced composites.

Acknowledgments

A portion of this research was sponsored by the User program of the High Temperature Material Laboratory of Oak Ridge National Laboratory and by National Science Foundation Grant 9983582 (Dr. K. P. Rajurkar, Program Director).

References

[1] ASTM D 638-99: Standard Test Method for Tensile Strength of Plastics, *Annual Book of ASTM Standards*, ASTM International, West Conshohocken, PA, 1999.

[2] Garrell, M. G., Ma, B. M., Lara-Curzio, E., Shih, A. J., and Scattergood, R. O., "Mechanical Properties of Nylon Bonded Nd-Fe-B Permanent Magnets," *Journal of Magnetism and Magnetic Materials*, accepted for publication.

[3] Garrell, M. G., Ma, B. M., Lara-Curzio, E., Shih, A. J., and Scattergood, R. O., "Mechanical Properties of Polyphenylene-Sulfide (PPS) Bonded Nd-Fe-B Permanent Magnets," *Materials Science and Engineering: A*, submitted.

[4] Garrell, M. G., *Mechanical Properties of Injection Molded Permanent Magnets*, M.S. thesis, North Carolina State University, Raleigh, NC, April 2002.

[5] Pilkey, W. D., *Peterson's Stress Concentration Factors*, 2nd ed., John Wiley & Sons, New York, 1997.

[6] Wilson, L. H. and White, D. J. "Stress-Concentration Factors for Shoulder Fillets and Grooves in Plates," *Journal of Strain Analysis*, Vol. 8, 1973, pp. 43–51.

[7] Frocht, M. M. "Factor of Stress Concentration Photoelastically Determined," *Transactions of ASME*, 1935, Vol. 57, pp. A-67–A-68.

[8] Worthem, D. W., *Flat Tension Specimen Design for Advanced Composites*, NASA Technical Report CR-185261, NASA Lewis Research Center, Cleveland, OH, 1990.

[9] Shi, J., Brady, L., and Ireson, A., "Design of Room Temperature Tension Specimen Made of Ceramic Matrix Composites," *Key Engineering Materials*, Vol. 164–165, Trans Tech Publications, 1999, pp. 257–260.

[10] Wang, Z, Chiang, C. K., and Chuang, T.-J., "Optimum Design of a Ceramic Tensile Creep Specimen Using a Finite Element Method," *Journal of Research of the National Institute of Standards and Technology*, Vol. 102, 1997, pp. 15–28.

[11] Oplinger, D. W., Parker, B. S., Gandhi, K. R., Lamothe, R., and Foley, G., "On the Streamline Specimen for Tension Testing of Composite Materials," *Recent Advances in Composites in the United States and Japan, ASTM STP 864,* J. R. Vinson and M. Taya, Eds., ASTM International, West Conshohocken, PA, 1985, pp. 532–555.

[12] McCrum, N. G., Buckley, C. P., and Bucknall, C. B., *Principles of Polymer Engineering*, 2nd ed., Oxford University Press, Oxford, 1997.

[13] Courtney, T. H., *Mechanical Behavior of Materials*, 2nd ed., McGraw-Hill, New York, 2000.